TECHNICAL MEMORANDUMS

NATIONAL ADVISORY COMMITTEE FOR AERONAUTICS

No. 573

AIR FORCES AND AIR-FORCE MOMENTS AT LARGE ANGLES OF ATTACK AND HOW THEY ARE AFFECTED BY THE SHAPE OF THE WING

By Richard Fuchs and Wilhelm Schmidt

From Zeitschrift für Flugtechnik und Motorluftschiffahrt
January 14, 1930

Washington
July, 1930

NATIONAL ADVISORY COMMITTEE FOR AERONAUTICS.

TECHNICAL MEMORANDUM NO. 573.

AIR FORCES AND AIR-FORCE MOMENTS AT LARGE ANGLES OF ATTACK AND HOW THEY ARE AFFECTED BY THE SHAPE OF THE WING.*

By Richard Fuchs and Wilhelm Schmidt.

S u m m a r y

The present report is, in the first place, a compilation of the test results now available from wing tests up to angles of attack of 90°. Reports are also given of tests with monoplane and auxiliary wings in the Göttingen wind tunnel for the purpose of plotting a steadily rising curve of the normal force as a function of the angle of attack.

The comparison of a series of typical wings shows that the single wing with auxiliary wing of Figure 24 greatly reduces the danger of spinning. This result is approached by the staggered biplane wing and by the monoplane wing, while the poorest results were obtained with the ordinary biplane wing.

In replacing the wing of a Junkers A 35 low-wing monoplane by the single wing with auxiliary wing of Figure 24, an investigation of the equilibrium of all the forces and moments about the airplane shows that the danger of spinning is completely eliminated.

---

*"Luftkräfte und Luftkraftmomente bei grossen Anstellwinkeln und ihre Abhängigkeit von der Tragwerksgestalt," the 168th report of the Deutsche Versuchsanstalt für Luftfahrt, Berlin-Adlershof. From Zeitschrift für Flugtechnik und Motorluftschiffahrt, January 14, 1930, pp. 1-12.

The monoplane wing of Figure 24 with the auxiliary wing set at a negative angle of 20°, which renders spinning impossible, has a greater drag and smaller lift at small angles of attack than the single wing. In this form it is therefore not adapted for ordinary flight.

However, in giving the auxiliary wing of Figure 21 a positive decalage of approximately 5°, the lift and drag become nearly equal to those of the single wing.

1. Notation

x Path axis in wind direction and in the plane of symmetry of wing.

y_1 Lift axis perpendicular to x and in plane of symmetry of wing.

f Fuselage axes in plane of symmetry of wing and parallel to plane of wing chord.

y Strut axis perpendicular to f and in plane of symmetry of wing.

The positive direction of all the axes is shown by the arrows in Figures 1 and 2.

g	(m/s^2)	Acceleration due to gravity.
γ	(kg/m^3)	Density of air.
$q=\frac{\gamma}{2g}v^2$	(kg/m^2)	Dynamic pressure.
F	(m^2)	Area.
b	(m)	Span.
$t=\frac{F}{b}$	(m)	Mean chord. According to the index o or u, these symbols apply either to the upper or to the lower wing.

a (m) Distance between the two wing chords located in the plane of symmetry and assumed to be parallel.

s (m) Stagger, distance between the leading edges of the two wings located in the same chord plane. It is positive when the leading edge of the upper wing is farther forward than that of the lower wing.

δ (o) Decalage, angle between the wing chords located in the plane of symmetry. It is positive when the angle of attack of the upper wing is larger than that of the lower wing.

z (m) Distance between the plane of symmetry and the wing element $t\,d\,z$ parallel to it.

r (m) Distance between the airplane C.G. projected on the chord plane of the lower wing and the leading edge.

h (m) Height of the airplane C.G. above the chord plane of the lower wing.

v (m/s) Air speed.

ω_x (1/s) Speed of rotation about the path axis x.

ω_{y_1} " " " " " " lift " y_1.

These are positive when acting clockwise about their respective axes, as viewed in the positive direction.

α (o) Angle of attack, angle between path axis x and fuselage axis f (Figs. 1 and 2).

$\Delta\alpha = 57.3 \arctan \frac{z\omega_x}{v}$ change in the angle of attack due to the rotation ω_x.

A (kg) $c_a = \frac{A}{qF}$ lift in the direction of the lift axis y_1, positive in the positive direction of y_1.

W (kg) $c_w = \frac{W}{qF}$ drag in the direction of the path axis x, positive in the negative direction of x.

N	(kg)	$c_n = \frac{N}{qF} = c_a \cos \alpha + c_w \sin \alpha$,	normal force in the direction of the strut axis y, positive in the positive direction of y.
T	(kg)	$c_t = \frac{T}{qF} = c_w \cos \alpha - c_a \sin \alpha$,	tangential force in the direction of the fuselage axis f, positive in the negative direction f.
K'	(mkg)	$R' = \frac{K'}{qFb}$	moment about the path axis x.
L'	(mkg)	$Q' = \frac{L'}{qFb}$	moment about the lift axis y_1.
K	(mkg)	$R = \frac{K}{qFb}$	moment about the fuselage axis f.
L	(mkg)	$Q = \frac{L}{qFb}$	moment about the strut axis y. All the moments are positive when they act anticlockwise in the positive direction about their respective axes.
M	(mkg)	$c_m = \frac{M}{qFt}$	moment about the leading edge. For biplanes about the biplane lower wing. It is positive when it reduces the angles of attack.

2. Purpose and Scope of the Investigation

In a work dealing with steady spins (L_2) (Reference 2)*, we have already shown that the designer can greatly reduce the danger of spins by giving suitable shapes to the wings. The danger of spins is completely eliminated when the moments about the fuselage axis f, caused by a rotation ω_x about the path axis x and chiefly due to the wing, are positive, i.e., working against a positive rotation ω_x. For instance, these moments are positive only when each wing element, within a given range of

*See Bibliography, page 19.

angles of attack from $\alpha = 0^{\circ}$ through 90°, exhibits, parallel to the plane of symmetry, a normal-force curve as a function of α (subsequently denoted as the c_n curve) which rises steadily with increasing angle of attack.

A very small number of test results of air forces and air-force-moment measurements have been hitherto available. This alone seems to warrant a closer survey of these results which will also be used for comparing the air forces and moments of a certain number of typical wings such as the monoplane wing, the ordinary and staggered biplane wing and lastly, the monoplane wing with auxiliary wing. All the values hitherto used for biplane wings were computed from English reports to which we shall refer repeatedly and which are listed in the bibliography at the end.

The influence of wing gap and decalage on the air forces and air-force moments of hitherto known biplane wings could not be taken into consideration for lack of test results at large angles of attack. We refer the reader to the English reports L_3, L_4, and L_5, which contain test results up to mean angles of attack. These measurements, made with the above-mentioned typical wings for large angles of attack through 90°, show that such wings do not fulfill the requirements for a steadily increasing c_n curve. This fact confirmed us in our intention to develop a wing with the most perfect possible continually increasing c_n curve which would probably render spinning impossible.

We have been guided by the idea that a suitable combination of two wings might permit of raising the c_n curve of a monoplane wing, which falls off within the range of mean angles of attack near the maximum lift, so far as to develop a steadily increasing c_n curve roughly applicable to any wing element parallel to the plane of symmetry. It was proposed to achieve this result by means of an auxiliary wing of the same span but of smaller chord, having, moreover, a certain degree of decalage with respect to the main wing. The proper wing shape could be determined only by tests which were conducted in the Göttingen wind tunnel and regarding which we shall report farther on.

3. Test Installation for the Determination of the Air-Force Moments about the Fuselage and Strut Axes Set Up by a Rotation ω_x about the Flight-Path Axis and of the Corresponding $\frac{b\omega_x}{2v}$ Values for Autorotation

The test installation is shown schematically in Figures 1 and 2. Two bearings (A and B) rigidly mounted in the wind tunnel carry the path axis x parallel to the air flow. At the front end of this axis, which is first struck by the air flow, the wing models are preferably secured at the center of gravity S of the airplane. These models are clamped at the proper angle of incidence α to the path axis x to which the desired number of revolutions is imparted by an electric motor. The moments K' and L' about the path axis x and the lift axis y_1 are measured by a suitable device.

When, after breaking the connection between the motor and the path axis, the air is blown against the wing at an angle of attack above that of maximum lift, the wing develops, of itself, or after receiving a more or less strong impulse, a rotation of gradually increasing speed which, after a certain while, becomes uniform and is called autorotation. The English report L_6 contains a good representation of such a test installation. The moments K and L about the fuselage and strut axes are still determined by conversion of the moments K' and L'. It would be very desirable to devise a test installation for the direct measurement of the moments K and L, which are extremely important for spin investigations.

4. Calculation of the Air-Force Moments about the Fuselage and Strut Axes Set up by a Rotation ω_x about the Flight-Path Axis and of the corresponding $\frac{b\omega_x}{2v}$ values of Autorotation. Comparison of the Calculated and Experimentally Found Values

For the calculation of the air-force moments the monoplane and biplane wings are assumed to be cut into the greatest possible number of elements $t\,d\,z$ or $(t_o + t_u)\,dz$ parallel to the plane of symmetry, the distance between these elements and the plane being z. Then, according to Figure 3, the moments R' and Q' of the monoplane wing develop about the path and lift axes, as a result of the rotation ω_x. They are also appli-

cable to biplane wings when $t_o + t_u$ is substituted for t and $F_o + F_u$ for F.

$$R' = \frac{1}{F\,b} \int_{z=-\frac{b}{2}}^{+\frac{b}{2}} [c_a (\alpha + \Delta\alpha) \cos \Delta\alpha + c_w (\alpha + \Delta\alpha) \sin \Delta\alpha] \frac{1}{\cos^2 \Delta\alpha}\, tz\,dz \qquad (1)$$

$$Q' = \frac{1}{F\,b} \int_{z=-\frac{b}{2}}^{+\frac{b}{2}} [c_w (\alpha + \Delta\alpha) \cos \Delta\alpha - c_a (\alpha + \Delta\alpha) \sin \Delta\alpha] \frac{1}{\cos^2 \Delta\alpha}\, tz\,dz \qquad (2)$$

where

$$\Delta\alpha = 57.3 \arctan \frac{z\,\omega_x}{v}.$$

For such wings, the lift and drag of which are assumed constant over nearly the whole span, the lift and drag of the whole wing are measured only for the strictly required number of angles of attack and plotted in c_a and c_w curves against α. The air-force coefficients of the integrals are computed from these curves. They are approximately applicable to all the wing elements.

The previously mentioned moments R' and Q' about the path axis x or the lift axis y_1 have been determined experimentally in England for several wing models. The angle of attack α and $\frac{b\omega_x}{2\,v}$ were given definite values. By plotting R' and

Q' against α and $\frac{b\,\omega_x}{2\,v}$, there are obtained Figures 18 and 19 in which the plain lines represent test values and the dash lines represent values obtained by calculation. There is a fairly good agreement between the curves determined by tests and those obtained by calculation. The moments R and Q about the fuselage and strut axes, plotted in Figures 16 and 17, can be calculated as follows from R' and Q' in Figure 4:

$$R = R' \cos\alpha + Q' \sin\alpha \qquad (3)$$

$$Q = Q' \cos\alpha - R' \sin\alpha \qquad (4)$$

These moments are obtained in a different way from the curves c_n and $c_t = f(\alpha)$ by means of the following integrals:

$$R = \frac{1}{F\,b} \int_{z=-\frac{b}{2}}^{+\frac{b}{2}} c_n (\alpha + \Delta\alpha) \frac{1}{\cos^2 \Delta\alpha}\, tz\,dz \qquad (5)$$

$$Q = \frac{1}{F\,b} \int_{z=-\frac{b}{2}}^{+\frac{b}{2}} c_t (\alpha + \Delta\alpha) \frac{1}{\cos^2 \Delta\alpha}\, tz\,dz \qquad (6)$$

where $$\Delta\alpha = 57.3 \arctan \frac{z\,\omega_x}{v}\,.$$

As shown below, these integrals may be, in general, solved in a simpler and more accurate way than the integrals 1 and 2. Figure 5 illustrates our method. It shows the distribution of the normal force over the wing span. Since the rotation ω_x causes the angle of attack $\alpha + \Delta\alpha$ to vary continuously by the

value $\Delta\alpha = 57.3 \arctan \frac{z\omega_x}{v}$ with increasing distance z from the plane of symmetry of the wing and the normal force of curve c_n corresponding to the angle of attack is obtained as a function of α, the curve $\frac{c_n}{\cos^2 \Delta\alpha}$, plotted against α in Figure 5 resembles, except for the factor $\frac{1}{\cos^2 \Delta\alpha}$, a more or less extended portion of the c_n curve for all values of α. Herein lies the advantage of the method in so far as it enables the $\frac{c_n}{\cos^2 \Delta\alpha}$ curve to be more easily and accurately plotted against α. The estimation of the integral is fully explained by Figure 5.

5. Comparison of the Air Forces and Air-Force Moments of the Following Wing Types Measured at Large Angles of Attack up to 90°:

   a) monoplane wing,
   b) ordinary biplane wings,
   c) staggered biplane wings,
   d) monoplane wing with auxiliary wing for different values of decalage, stagger and gap

The values of the lift, drag and moment about the leading edge, as measured in the wind tunnel, are always plotted against the angle of attack. The flow about a series of wings separates suddenly at angles of attack slightly above the maximum lift. Two measurements were made within this critical range for each setting of the angle of attack, in order to check its variation from larger or from smaller values. The true magnitude of these values is not accurately known for full-sized airplanes. The values of the separated flow will probably have to be taken

into consideration on the assumption that the separation does not take place suddenly but gradually, especially with a rotation about the path axis. The c_n curve was therefore plotted so as to establish a gradual relation between the values of the definitely separated flow and those of the definitely adhering flow. The normal and tangential forces were calculated by the formulas $c_n = c_a \cos\alpha + c_w \sin\alpha$ and $c_t = c_w \cos\alpha - c_a \sin\alpha$ and plotted, together with the above values, against the angle of attack. The calculation of the moments about the fuselage axis was based in most cases on the c_n curve by means of equation (5). They were all plotted in diagrams against the angle of attack and $\frac{b\omega_x}{2v}$. The α and $\frac{b\omega_x}{2v}$ values of autorotation about the fuselage axis, plotted as curves in Figure 37, can be taken as the zero points of these diagrams.

a) Monoplane Wing

The measurements were made in the Göttingen wind tunnel with two normal wings of 1 m span and 0.2 m chord. One of the normal wings had the normal Göttingen 423 section of Figure 6 and the other roughly that of Figure 9. Figures 7 and 10 show the corresponding test results.

b) Ordinary Biplane Wings

The test results of Figure 12 are taken from the English reports L_7 and L_8. The tests were made with an ordinary biplane wing of 1.28 m span and 0.43 m² total area, the section of which was obtained from the English reports L_8 and L_9 and is represented in Figure 11.

c) Staggered Biplane Wings

The test results shown in Figure 15 were taken from the English report L_{10}. They apply to staggered biplane wings of 1.2 meter span and 0.38 square meter total area, whose profile was taken from the English reports L_{11} and L_{12}, as represented in Figure 14.

The English report L_{10} also contains data on the measured and calculated moments R' and Q' about the path and the lift axes which are plotted in Figures 18 and 19. Figures 16 and 17 show the moments R and Q about the fuselage and strut axes, as obtained by calculation with the aid of formulas (3) and (4).

With the moments about the path axis balanced, the corresponding α and $\frac{b\omega_x}{2v}$ values are obtained from the zero points of the curves in Figure 18. These $\frac{b\omega_x}{2v}$ values of autorotation about the path axis are plotted in Figure 20 against the angle of attack. The same figure likewise contains the values of the English report L_{10} which were determined by autorotation tests. The $\frac{b\omega_x}{2v}$ values determined by tests and those obtained by calculation agree fairly well when mean figures are taken for the values measured during positive and negative rotations ω_x. Furthermore, for small $\frac{b\omega_x}{2v}$ values, autorotation about the path axis develops only when

$$\frac{d\, c_a}{d\, \alpha} + c_w < 0.$$

d) Monoplane Wing with Auxiliary Wing

All the measurements, the results of which are plotted in Figures 27 to 32, were conducted in the Göttingen wind tunnel with the wings shown in Figures 21 to 26. The monoplane wing had a span of 1 meter and a chord of 0.2 meter. The auxiliary wing, of the same span, had a chord of only 0.07 meter.

6. Comparison of the Different Wings

As shown in Figure 35, the lift of the monoplane wing with the auxiliary wing of Figure 24 agrees, at small angles of attack, with that of the ordinary biplane wings and of the staggered biplane wings of Figures 11 and 14. All these wings have considerably smaller lift values than the monoplane wing of Figure 6.

For $\alpha = 6.5^{\circ}$ the drag of the monoplane wing with auxiliary wing has just the same value as that of the single monoplane wing, while it is much larger at small angles of attack. On the other hand, the drag of the ordinary and of the staggered biplane wings is much smaller.

At mean and large angles of attack, the lift of the monoplane wing with auxiliary wing is much greater than that of all the other wings with nearly the same c_n curves. Its drag is almost the same as that of the monoplane wing, while for $\alpha = 90^{\circ}$, it reaches nearly twice the value of the drag of the ordinary biplane wing. When the air is strongly blown from below

against the biplane wings, the upper wing is screened by the lower wing (L_{13}) to an extent which increases with decreasing stagger. For this reason, the drag of nonstaggered biplane wings must be particularly small.

The c_n curve nearly coincides with the c_a curve at small angles of attack and with the c_w curve at large angles of attack. According to Figure 34, the c_n curve of the monoplane wing with auxiliary wing increases quite steadily. Furthermore, within a small range of angles of attack above the maximum lift, the c_n curve of the staggered biplane wing drops but little, that of the ordinary biplane wing slightly more, and that of the monoplane wing much more, only to rise again at large angles of attack. The normal force of the ordinary biplane wing decreases considerably at angles of attack above 40°.

The moments about the leading edge are plotted in Figure 36. The moment of the monoplane wing with auxiliary wing is smaller than that of the single monoplane wing, but much greater than that of the ordinary and of the staggered biplane wing. The moments about the fuselage axis are plotted in Figures 8, 13, 16, and 33 against α and $\frac{b\omega_x}{2V}$ for the corresponding wings. The corresponding α and $\frac{b\omega_x}{2V}$ values of autorotation about the fuselage axis, as plotted in Figure 37, were obtained from the zero points of the moment curves.

The monoplane wing with auxiliary wing can autorotate only within a very small range of relatively large angles of attack.

The corresponding range of the staggered biplane wing is materially greater and begins at much smaller angles of attack. Autorotation of the single monoplane wing and of the ordinary biplane wing begins at still smaller angles of attack and covers a very wide range, which is widest for the ordinary biplane wing. A test of the wing for the maximum $\frac{b\omega_x}{2V}$ values shows, according to Figure 37, that the monoplane wing with auxiliary wing has the smallest and the ordinary biplane wing the largest maximum value.

In Figure 38 the maximum values of the negative moments about the fuselage axis corresponding to the respective angles of attack, namely, the minimum values of the R curves, are plotted in new diagrams against $\frac{b\omega_x}{2V}$ and α. It now becomes apparent how much the monoplane wing with auxiliary wing differs from all the other wings. While the others have rather large negative moments, the corresponding moments of the monoplane wing with auxiliary wing are negligibly small.

The monoplane wing with auxiliary wing was specially tested for decalage, stagger, and gap. Figures 39 and 40 show the influence of decalage. At small angles of attack in normal flight the lift is increased with increasing decalage between the auxiliary and the monoplane wing. Since, according to Figure 9, the monoplane wing was tested without the honeycomb, the measured lift values are probably too large. Hence, at small angles of attack and for a positive decalage of the auxiliary wing of

about 5°, the lift of the monoplane wing is nearly equaled. The drag of the monoplane wing with auxiliary wing is smallest and equal to that of the single monoplane wing at small angles of attack and for a slightly negative decalage of the auxiliary wing of approximately 5°. The drag increases gradually when the auxiliary wing is deflected from this position in either direction. For a positive decalage of approximately 5° it is still nearly equal to that of the monoplane wing.

In reducing the wing gap or stagger, as shown in Figures 41 to 44, the maximum lift is increased and shifted toward larger angles of attack. At small angles of attack the lift and drag are scarcely changed by a variation of the wing gap or stagger.

In comparing the tested monoplane wings with auxiliary wings it appears that the wing with approximately -20° decalage of the auxiliary wing, best suited to prevent spinning, is not suitable for normal flight at small angles of attack. It may, however, be adapted to this purpose by giving the auxiliary wing a decalage of approximately +5°. The auxiliary wing should therefore be adjustable over at least one-third of its outer portion. Besides, much better results are obtained by changing the section and the chord of the auxiliary wing.

7. Change in the Equilibrium of All the Forces and Moments Acting on a Junkers A 35 Low-Wing Monoplane when Its Standard Wing is Replaced by the Wing Shown in Figure 24

The following investigation is a sequel to our study of the steady spin (L_2). It contains an explanation of the symbols used. As shown in Figure 45, all the c_a and c_w values of the whole airplane are greatly changed by the substitution of the monoplane wing with auxiliary wing of Figure 24 for the Junkers A 35 low-wing monoplane. Also, according to Figure 46, the moment about the spar axis is changed, but this change is probably offset by a corresponding deflection of the elevator, so that the curve of the original airplane holds good without any material variation.

The R_F moments about the fuselage axis, chiefly due to the wing, are determined for the single monoplane wing with auxiliary wing in exactly the same way as in the above work and plotted in Figure 47 against the angle of attack and the angle of glide. The α and φ values, for which the moments about the fuselage axis are balanced when all the forces about the airplane are in equilibrium, are derived from the zero points of the above curves. These values are plotted in Figure 48 with the curve d_1. Even with no aileron moment R_K a curve d can be plotted which, however, extends over only a small range of angles of attack and reaches gliding angles not exceeding a maximum value of -60°. It is rather far from all the b

curves including those plotted for strong "pulls" on the stick and designed to balance the moments about the spar axis.

In plotting, over all α values, constant positive or negative aileron moments R_K which throw the airplane in or out of banks during positive rotations ω, the abscissa of the curves plotted in Figure 47 must be shifted upward or downward parallel to itself. The α and φ values of the new zero points are also plotted in the d curves of Figure 48 with the parameter R_K. No d curve can be plotted for very small negative aileron moments which are possible at all angles of attack. There can be, therefore, no equilibrium of the moments about the fuselage axis in curvilinear flight.

Since even the aileron moment $R_{K\,max}$ of maximum aileron deflection decreases with increasing angle of attack, very definite maximum aileron moments can be reached only within a limited range of angles of attack. The d curves plotted in Figure 48 against the constant aileron moment have, therefore, an upper limit to the angle of attack. Above this limit the moments can be no longer balanced and it becomes impossible to keep the airplane in a banked position.

The d curves of certain aileron moments cut the b curves of certain elevator moments E_H in such a manner that steady spiral flight becomes possible, if the moments about the strut axis are also balanced for the α and φ values of the points of intersection. Steady spiral flights do not resemble spins. They may be rather steep but they only require a very strong

aileron moment, and the corresponding angle of attack does not exceed that of maximum lift. Besides, even the slightest change in the aileron moment greatly disturbs the conditions of equilibrium. They differ in no way from ordinary spiral flights.

If a spin is considered as a very steep spiral flight at angles of attack above the maximum lift and, contrary to the ordinary spiral flight, with very small aileron moments, possibly zero, the above considerations show that a spin, thus defined, is not possible with an airplane equipped with the wing of Figure 24.

9. Bibliography

1. Fuchs and Hopf : "Aerodynamik." R. C. Schmidt & Co., Berlin W 62, 1922.

2. Fuchs, R. and Schmidt, W. : "Stationärer Trudelflug," D.V.L. Report 117, Luftfahrtforschung, Vol. III (1929), p. 1; D.V.L. Yearbook, 1929, p. 157.

3. Glauert, H. : "The Investigation of the Spin of an Aeroplane." British A.C.A. R&M No. 618 (1919).

4. Irving, H. B. and Batson, A. S. : "Preliminary Note on the Effect of Stagger and Decalage on the Autorotation of an R.A.F. 15 Biplane." British A.R.C. R&M No. 733 (1920).

5. Bradfield, F. B. : "Lateral Control of Bristol Fighter at Low Speeds. Measurement of Rolling and Yawing Moments of Model Wings Due to Rolling." British A.R.C. R&M No. 787 (1921).

6. Cowley, W. L. and Lock, C. N. H. : "A Comparison between the Aerodynamic Properties of Two Aerofoils of the Same Section, but with Square and Rounded Wing Tips Respectively." British A.R.C. R&M No. 816 (1921).

7. Cowley, W. L. and Jones, L. J. : "Biplane Investigation with R.A.F. 15 Section. Part II: British A.R.C. R&M No. 857 (1922).

8. Cowley, W. L. Gadd, A. G., Jones, L. J., and Skan, Sylvia W. : "Biplane Investigation with R.A.F. 15 Section. Part III: Tests at Various Staggers and Gap Chord Ratios." British A.R.C. R&M No. 872 (1923).

9. Relf, E. F. and Ower, E. : "Lift, Drag and Pitching Moment of the 1/5th Scale Bristol Fighter Model in the Duplex Wind Tunnel." British A.R.C. R&M No. 876 (1923).

10. Lavender, T. : "A Continuous Rotation Balance for the Measurement of Pitching and Yawing Moments Due to Angular Velocity of Roll (M_p and N_p)." British A.R.C. R&M No. 936 (1925).

11. Bradfield, F. B. : "Pitching and Yawing Moments with Sideslip on a Model Aeroplane with Zero Stagger." British A.R.C. R&M No. 965 (1925).

12. Bradfield, F. B. and Coombs, L. P. : "Autorotation Measurements on a Model Aeroplane with Zero Stagger." British A.R.C. R&M No. 975 (1925).

13. Loeser, Jr., Oscar E. : "Pressure Distribution Tests on PW-9 Wing Models from -18° through 90° Angle of Attack." N.A.C.A. Technical Report No. 296 (1929).

Translation by
National Advisory Committee
for Aeronautics.

Figs.1,2,3,4.

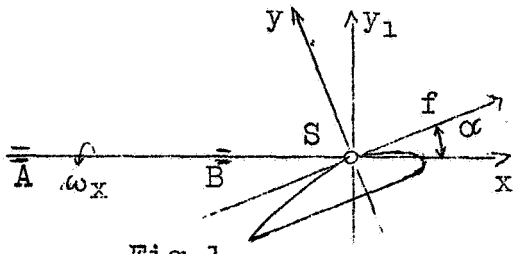

Fig.1
Schematic representation of the test installation.

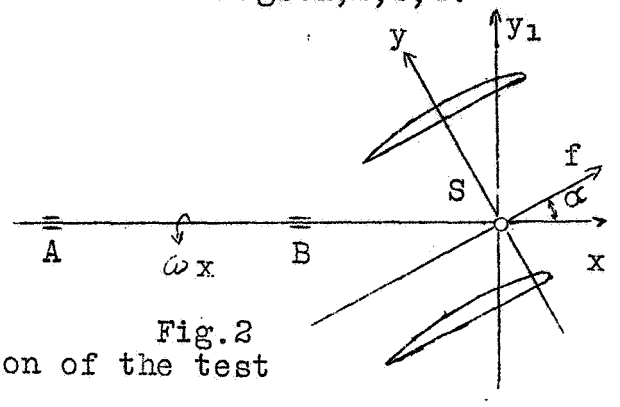

Fig.2

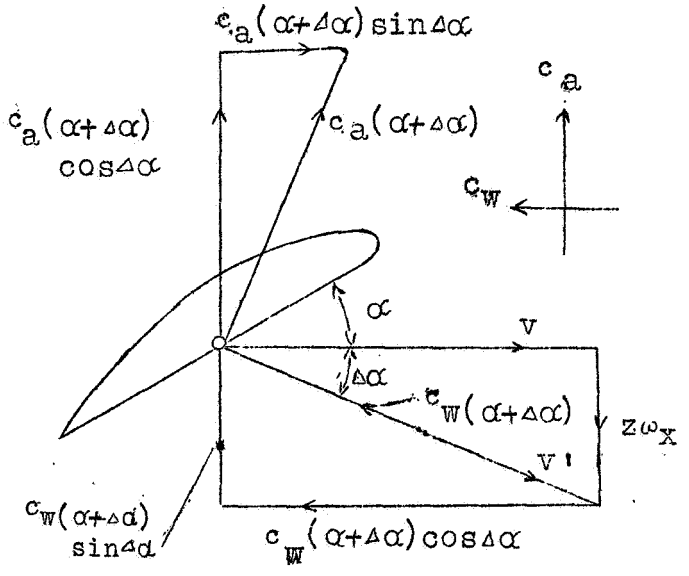

Fig.3 Lift, drag and variation of the angle of attack due to the rotation of a wing element about path axis parallel to the plane of symmetry.

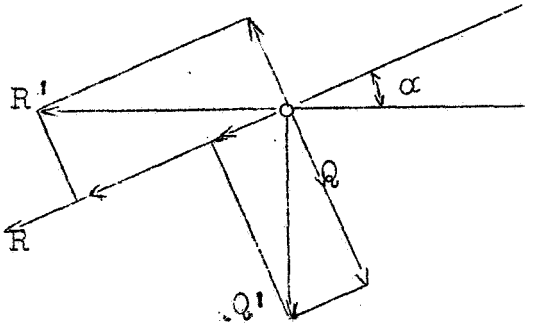

Fig.4
For the conversion of the moments about the path and lift axes to moments about the fuselage and strut axes..

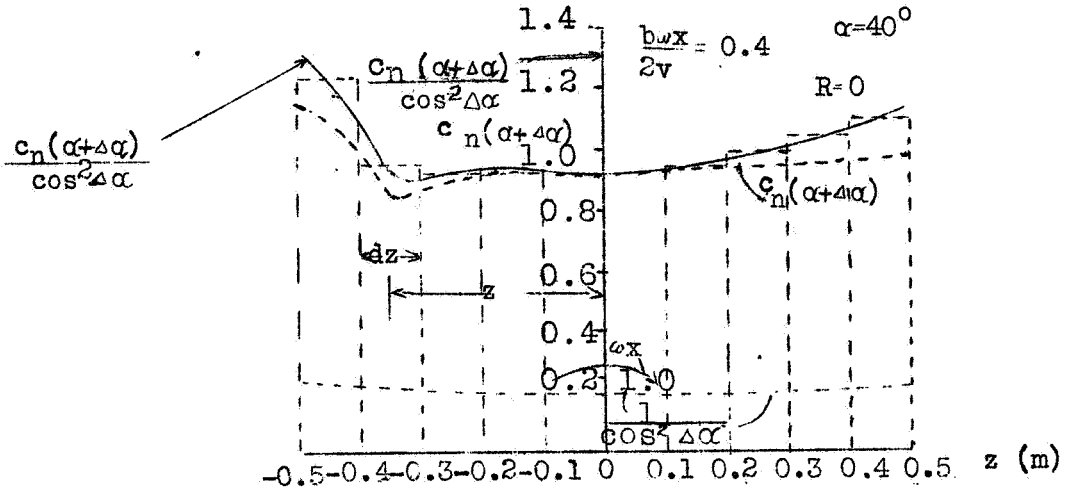

Fig.5 Example of air-force distribution over the wing.

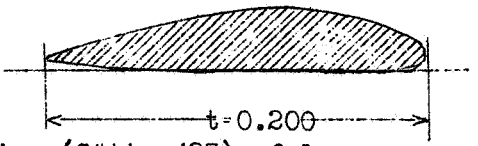

Fig.6 Monoplane wing (Gött. 423) of 1 m span and 0.2 m^2 area.

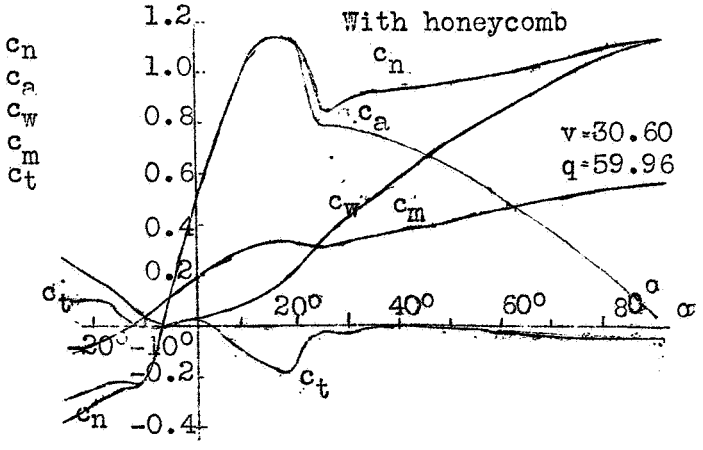

Fig.7 Lift, drag, moment about the leading edge, normal and tangential forces plotted against the angle of attack of the monoplane wing of Fig.6.

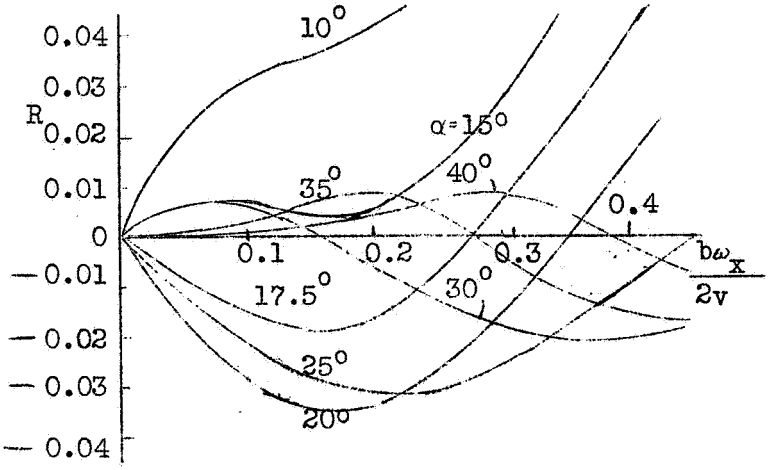

Fig.8 Calculated moment about the fuselage axis plotted against the angle of attack and $\frac{b\omega x}{2v}$ for the monoplane wing of Fig.6.

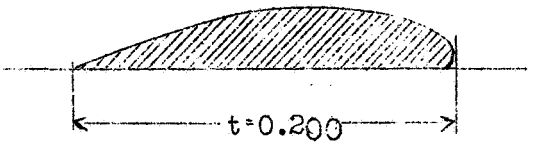

Fig.9 Profile of monoplane wing of 1 m span and 0.2 m^2 area.

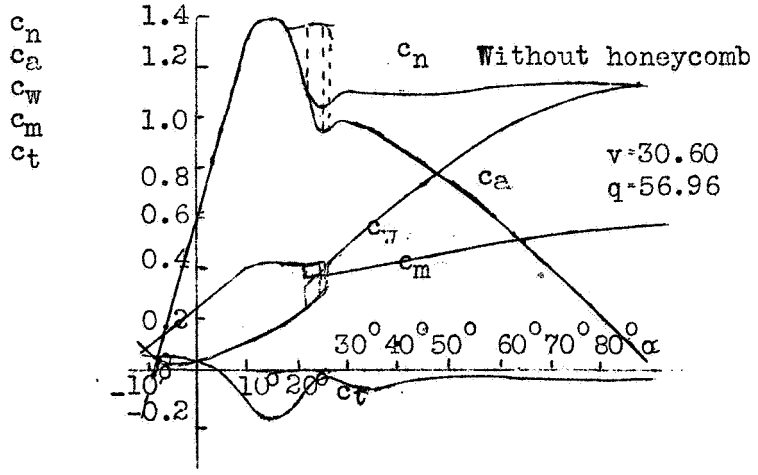

Fig.10 Lift, drag, moment about the leading edge, normal and tangential forces plotted against the angle of attack of monoplane wing of Fig.9.

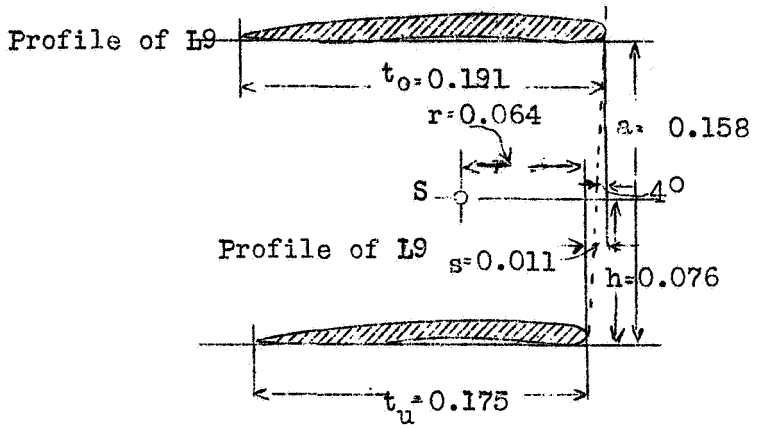

Fig.11 Profile of the ordinary biplane wing of 1.28 m span and 0.43 m^2 total area. S is the C.G. of the airplane.

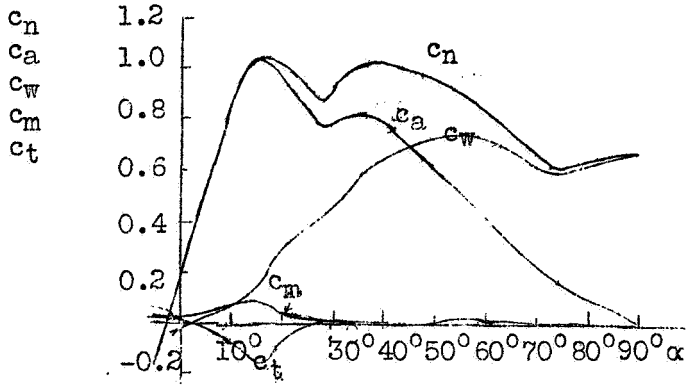

Fig.12 Lift, drag, moment about the leading edge, normal and tangential forces plotted against the angle of attack for the ordinary biplane wing of Fig.11.

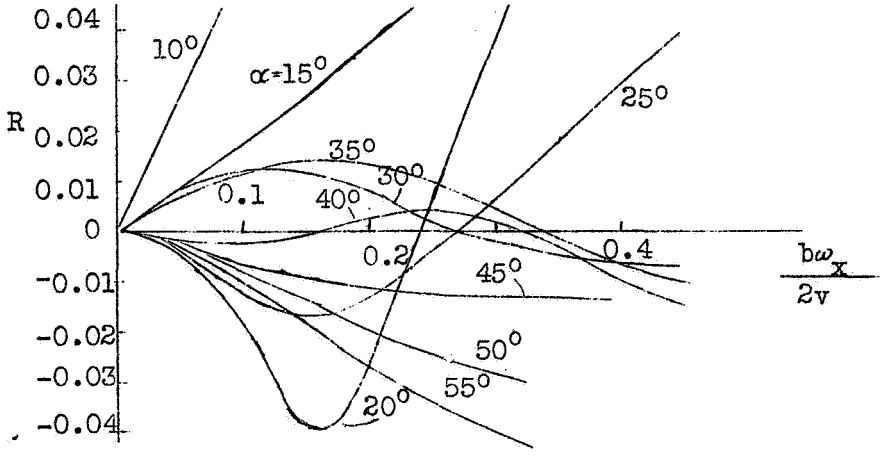

Fig.13 Calculated moment about the fuselage axis plotted against the angle of attack and $\frac{b\omega x}{2v}$ for the ordinary biplane wing of Fig.11.

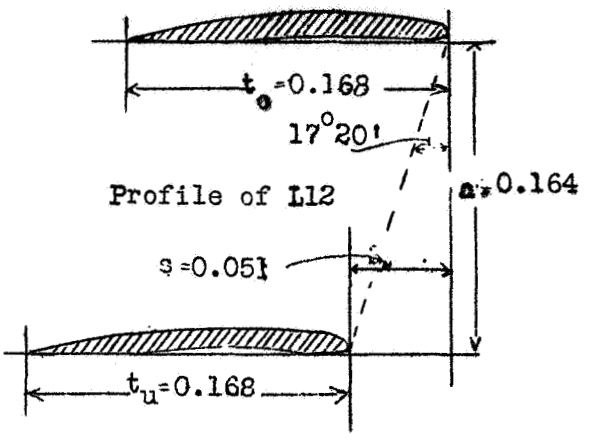

Fig.14 Profile of the staggered biplane wings of 1.2 m span and 0.38 m^2 total area.

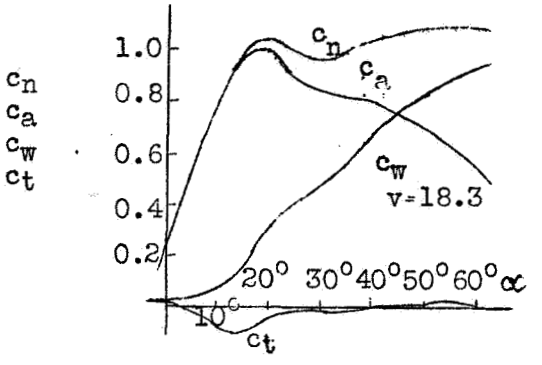

Fig.15 Lift, drag, normal and tangential forces plotted against the angle of attack for the staggered biplane wing of Fig.14.

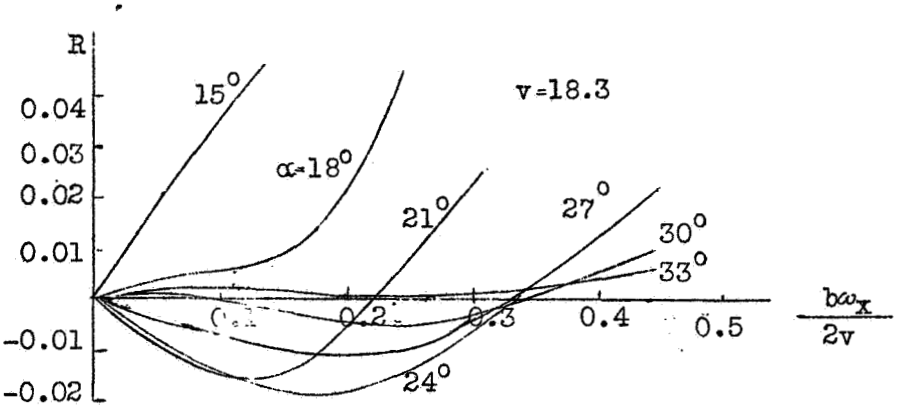

Fig.16 Moment about the fuselage axis plotted against the angle of attack and $\frac{b\omega x}{2v}$ for the staggered biplane wing of Fig.14.

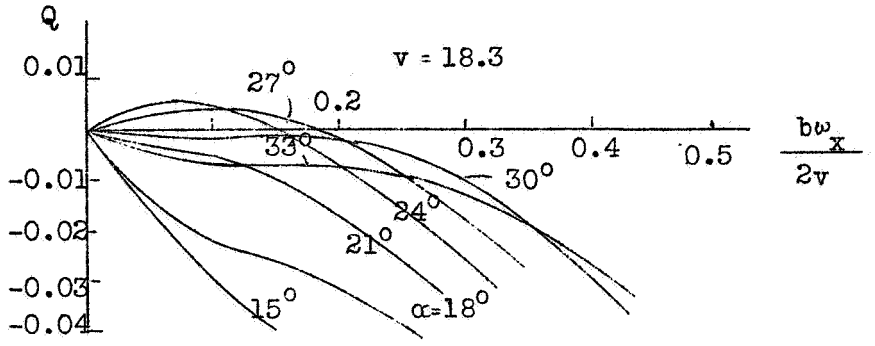

Fig.17 Moment about the strut axis plotted against the angle of attack and $\frac{b\omega x}{2v}$ for the staggered biplane wing of Fig.14.

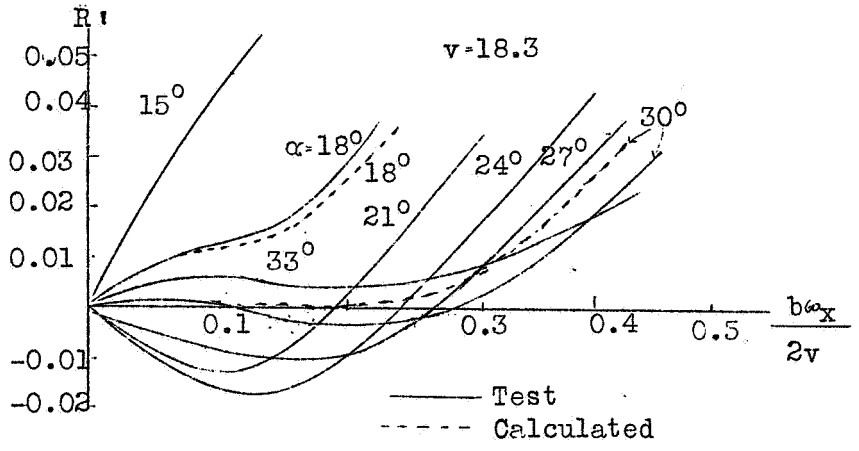

Fig.18 Moment about the path axis plotted against the angle of attack and $\frac{b\omega x}{2v}$ for the staggered biplane wing of Fig.14.

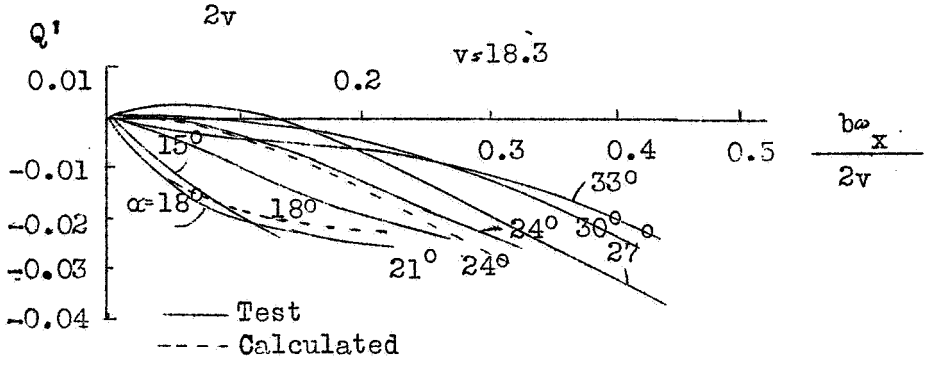

Fig.19 Moment about the lift axis plotted against the angle of attack and $\frac{b\omega x}{2v}$ for the staggered biplane wing of Fig.14.

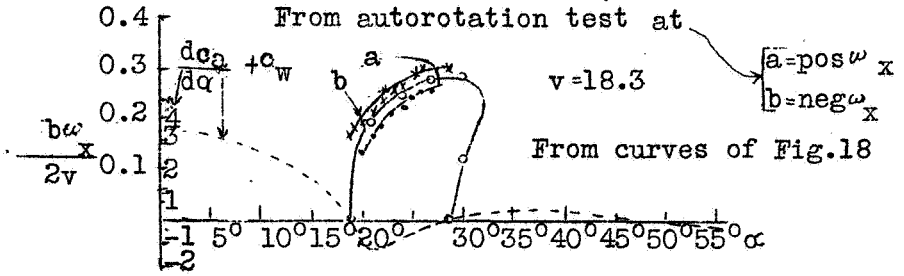

Fig.20 $\frac{b\omega_x}{2v}$ values of autorotation about the path axis and $\frac{dc_a}{d\alpha}+c_w$ values plotted against the angle of attack for the staggered biplane wing of Fig.14.

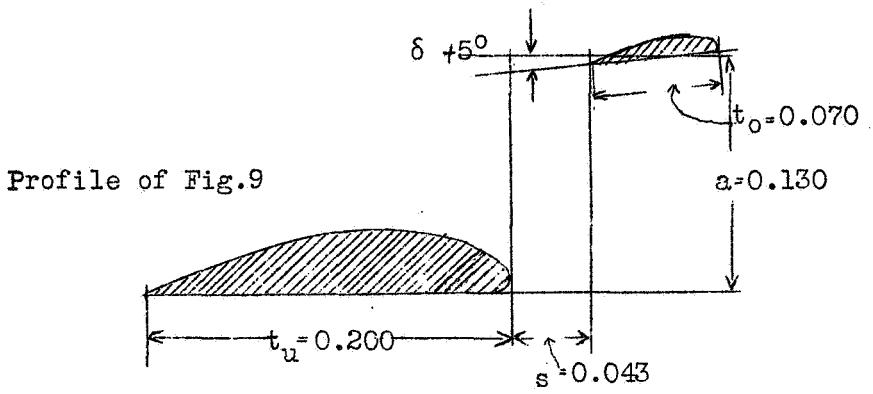

Fig.21. Profile of monoplane wing with auxiliary wing of 1 m span and 0.27 m^2 total area.

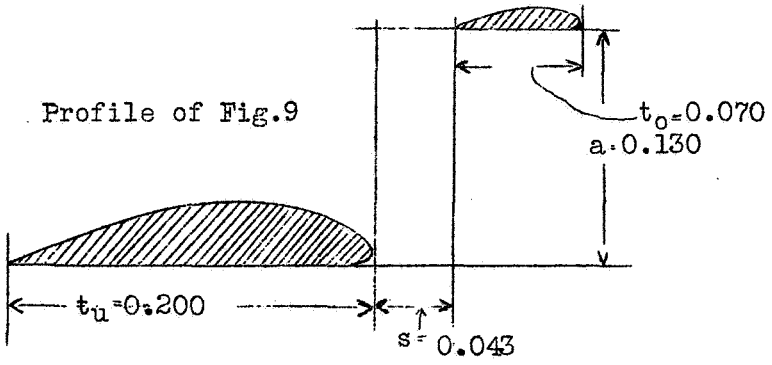

Fig.22 Profile of monoplane wing with auxiliary of 1 m span and 0.27 m^2 total area.

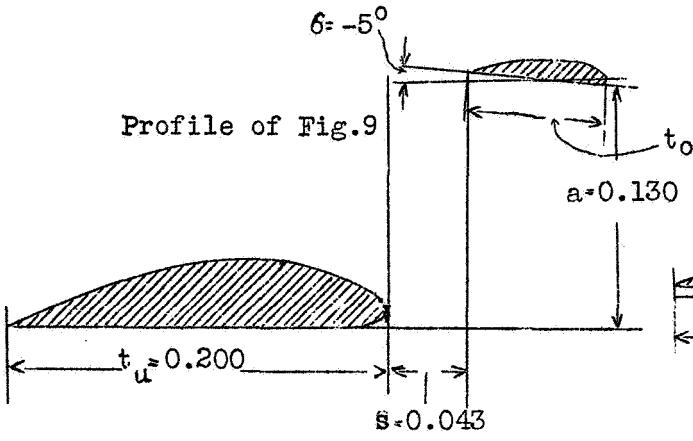

Fig.23

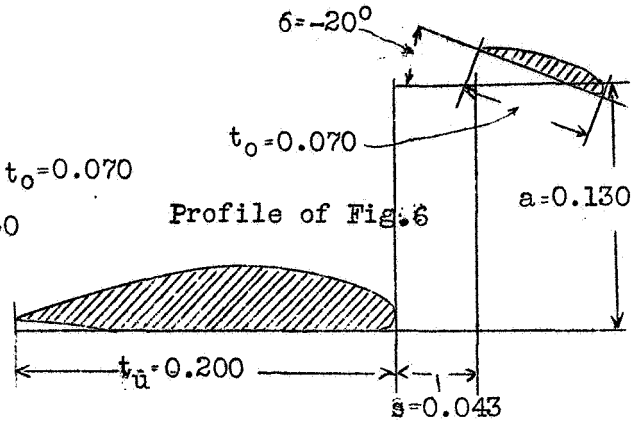

Fig.24

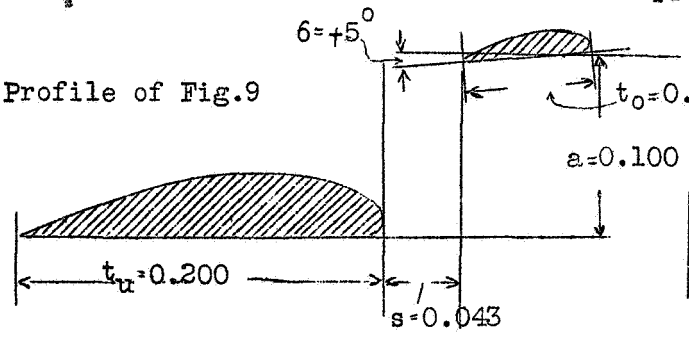

Fig.25

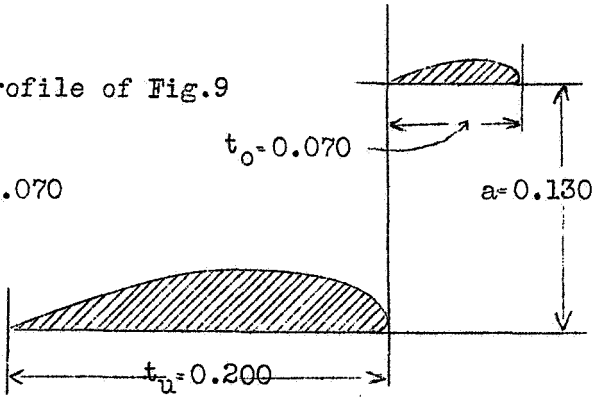

Fig.26

Profile of monoplane wing with auxiliary wing of 1 m span and 0.27 m^2 total area.

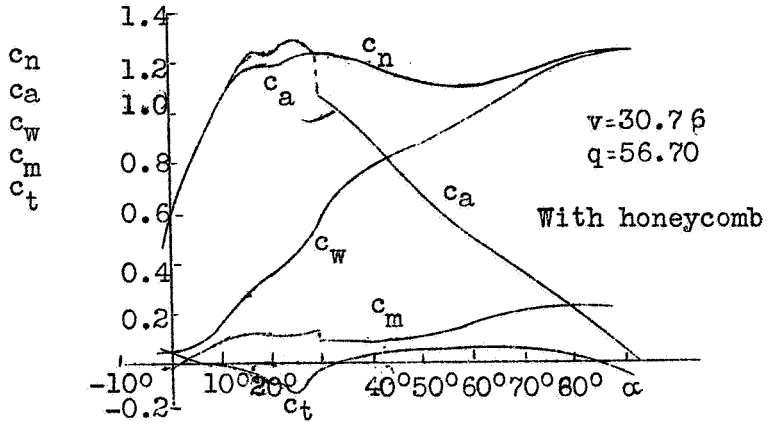

Fig.27 Wing of Fig.21

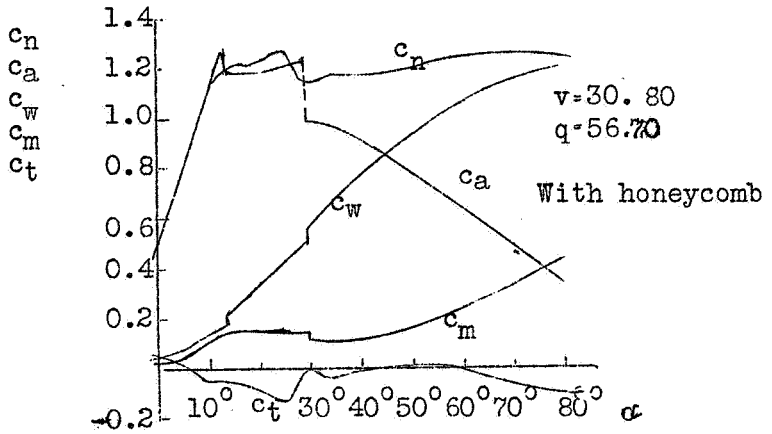

Fig.28 Wing of Fig.22

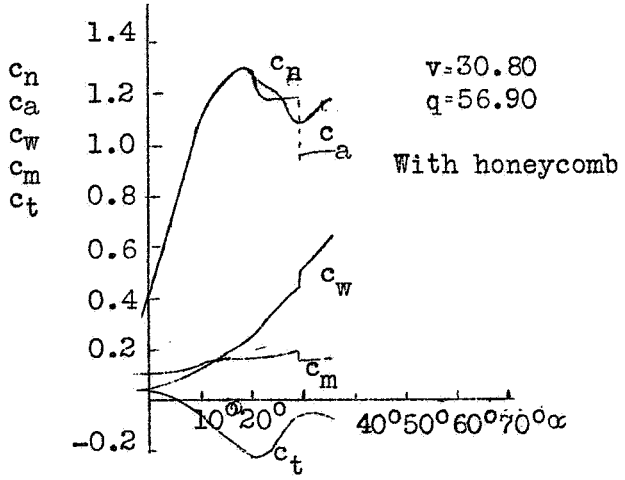

Fig.29 Wing of Fig.23.
Lift, drag, moment about leading edge, normal and tangential force of the different wings.

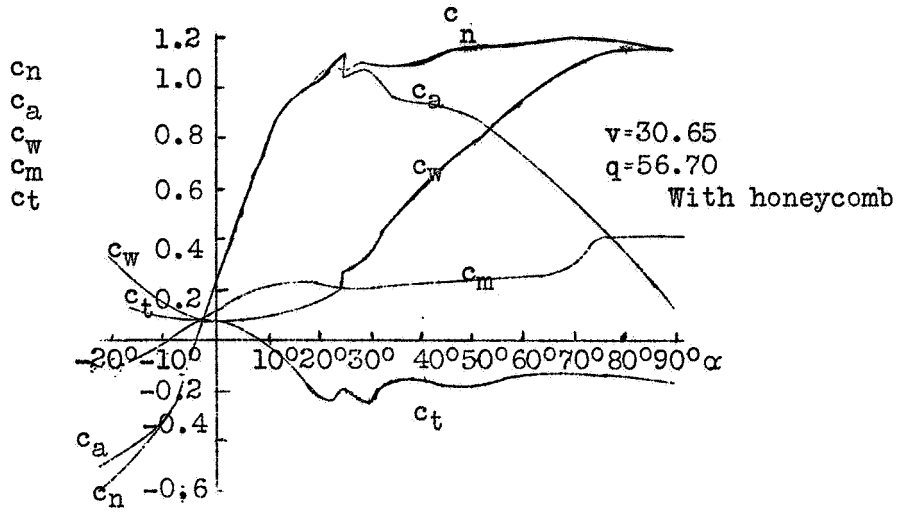

Fig.30 Wing of Fig.24

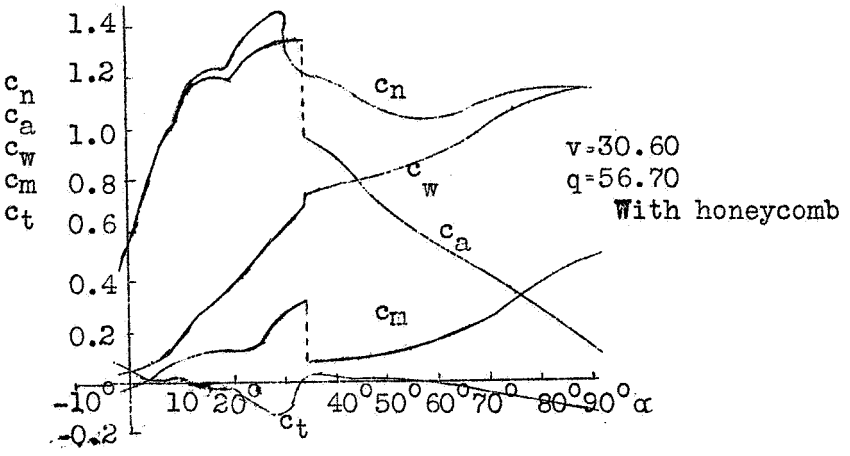

Fig.31 Wing of Fig.25.

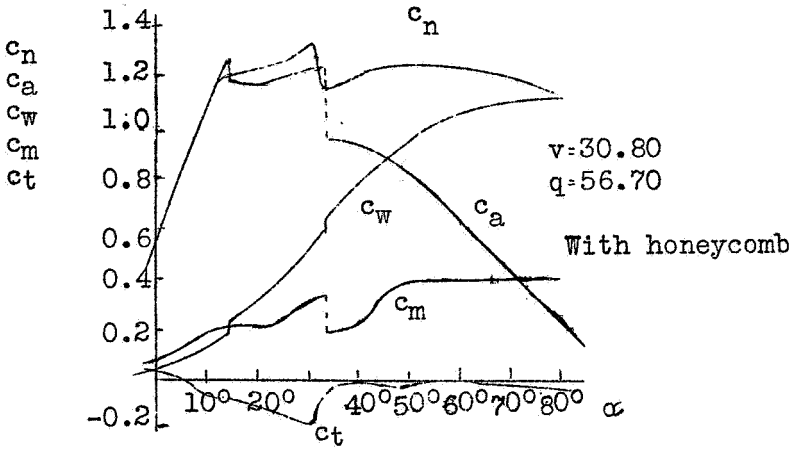

Fig.32 Wing of Fig.26.
Lift, drag, moment about leading edge, normal and tangential force of the different wings.

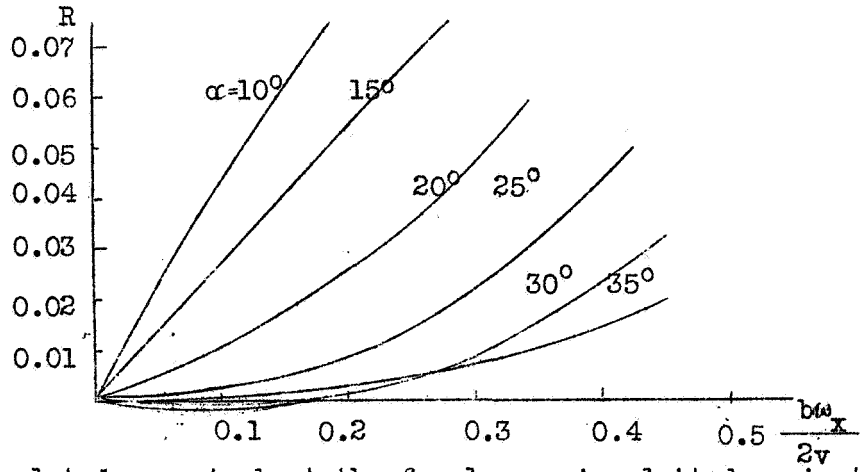

Fig.33 Calculated moment about the fuselage axis plotted against the angle of attack and $\frac{b\omega x}{2v}$ for the monoplane wing with auxiliary wing of Fig.24.

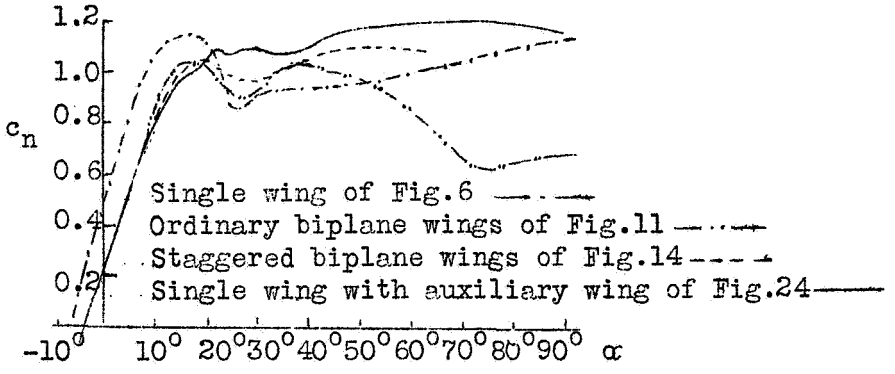

Fig.34 Normal force plotted against the angle of attack.

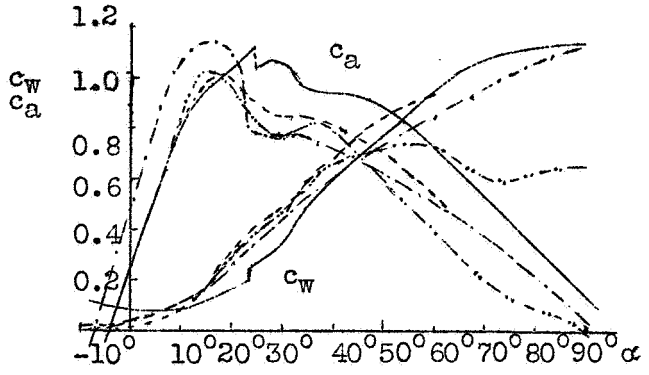

Fig.35 Lift and drag plotted against the angle of attack for the wings of Fig.34.

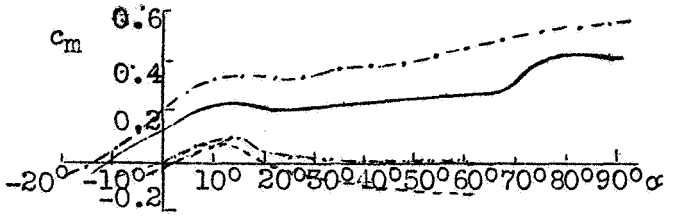

Fig.36 Moment about the leading edge plotted against the angle of attack for the wings of fig.34.

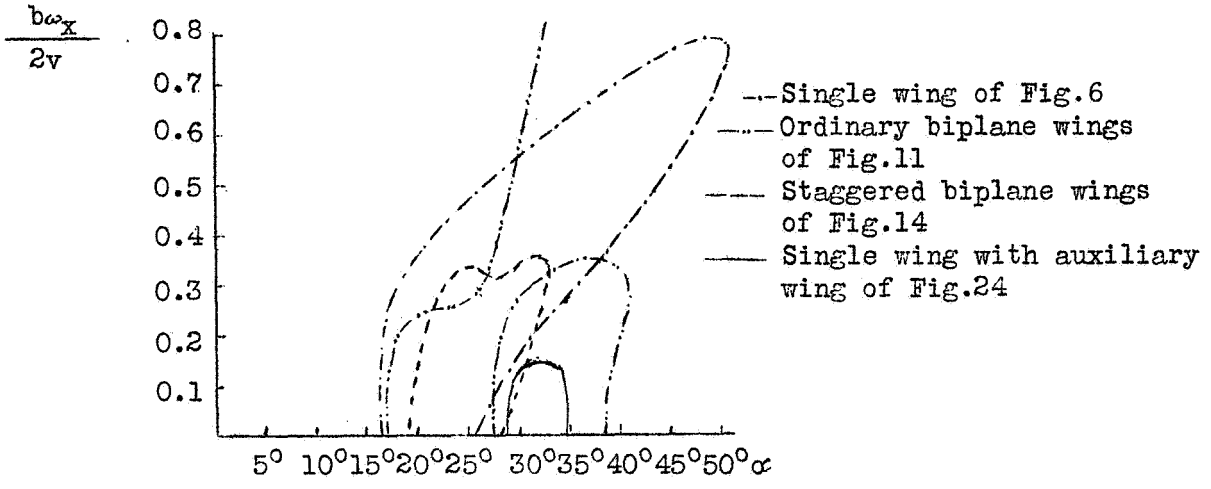

Fig.37 The $\frac{b\omega_x}{2v}$ values of autorotation about the fuselage axis plotted against the angle of attack.

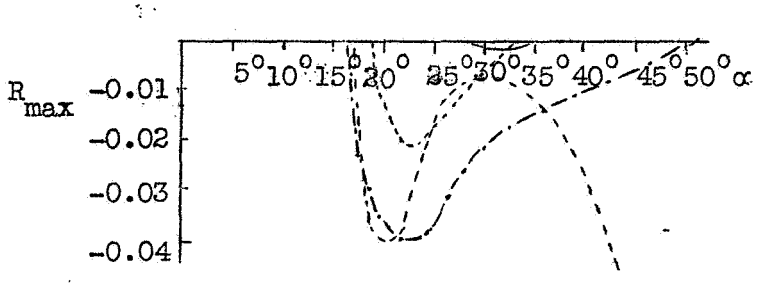

Fig.38 The maximun negative moments about the fuselage axis plotted against the angle of attack for the wings of Fig.37.

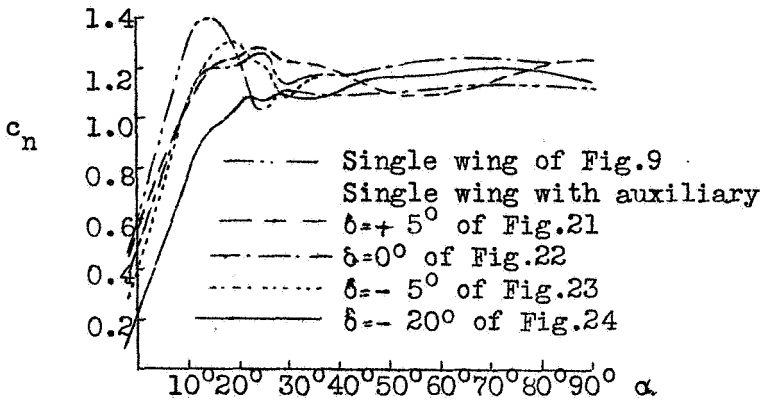

Fig.39 Normal force plotted against the angle of attack and decalage.

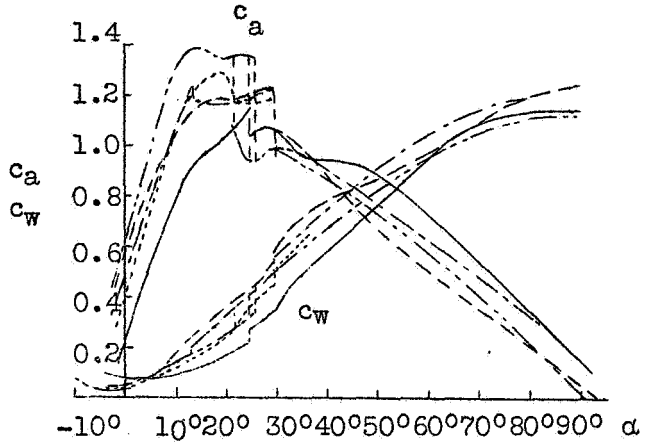

Fig.40 Lift and drag plotted against the angle of attack and decalage for the wings of Fig.39.

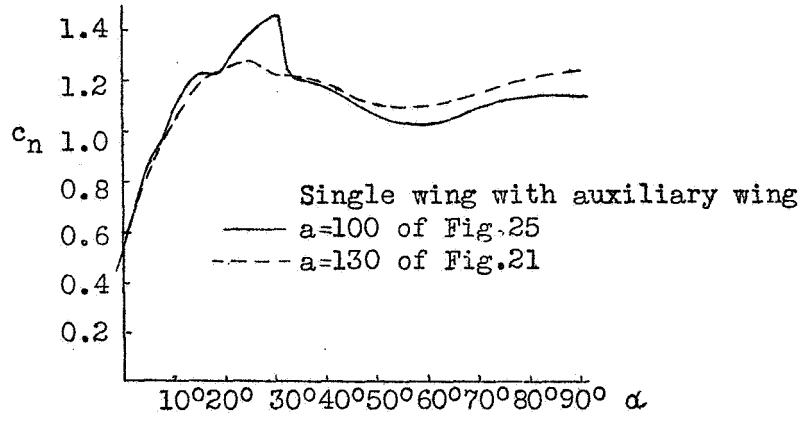

Fig.41 Normal force plotted against the angle of attack and the wing gap.

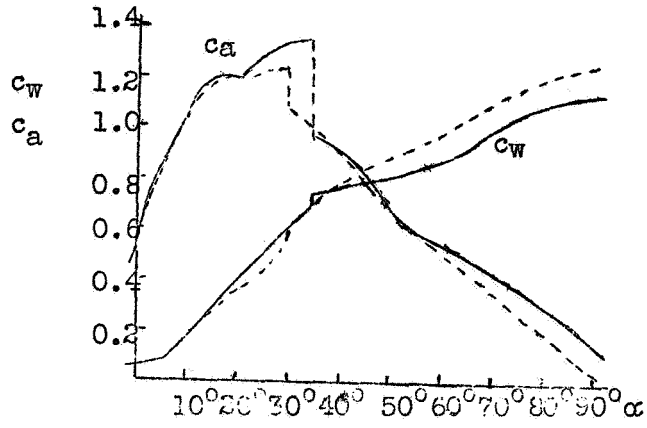

Fig.42 Lift and drag plotted against the angle of attack and the wing gap for the wings of Fig.41.

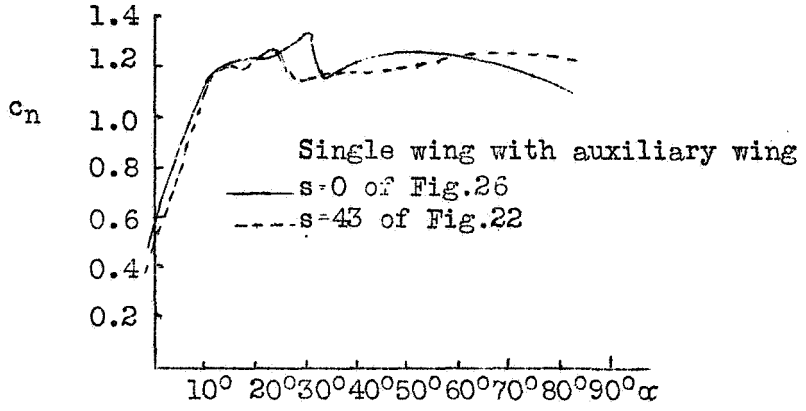

Fig.43 Normal force plotted against the angle of attack and the stagger.

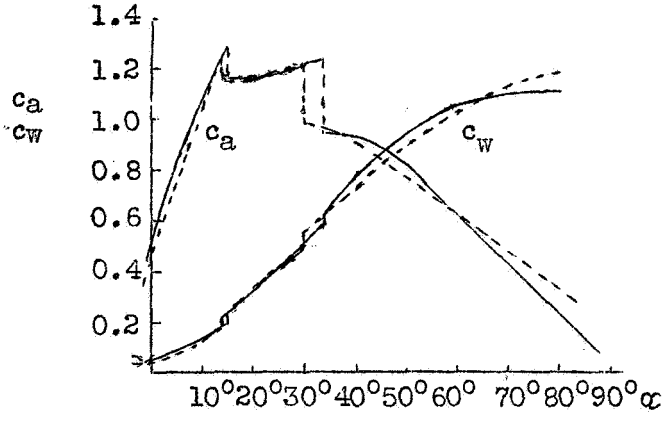

Fig.44. Lift and drag plotted against the angle of attack and the stagger for the wings of Fig.43.

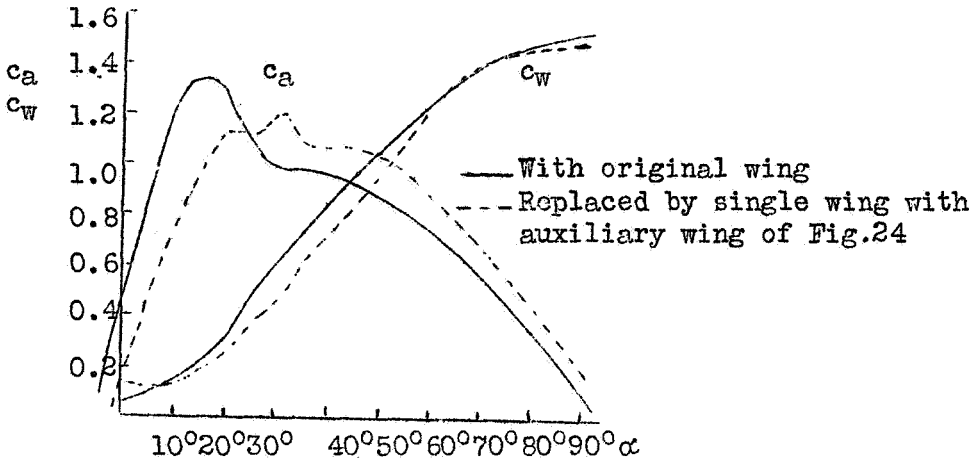

Fig.45 Lift and drag of a Junkers type A 35 low-wing monoplane plotted against the angle of attack.

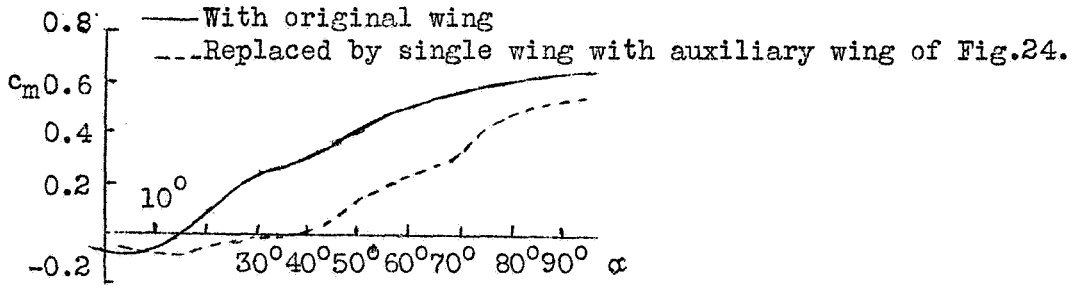

Fig.46 Moments about the spar axis of a Junkers type A 35 low-wing monoplane plotted against the angle of attack.

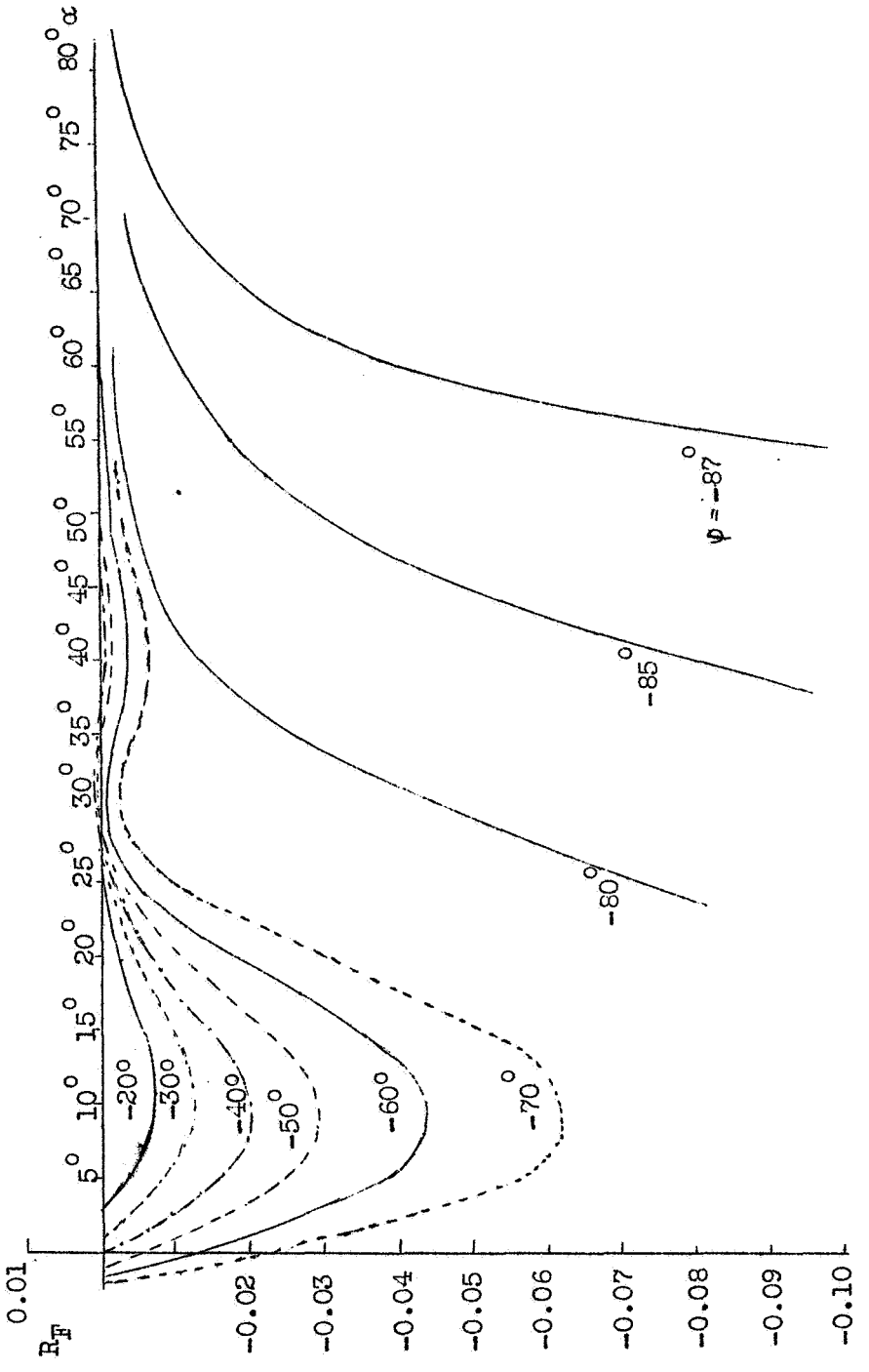

Fig.47 Air-force moment about the fuselage axis of a Junkers A 35 low-wing monoplane (original monoplane wing replaced by a single wing with auxiliary wing according to Fig.24) plotted against the angle of attack and the angle of glide.

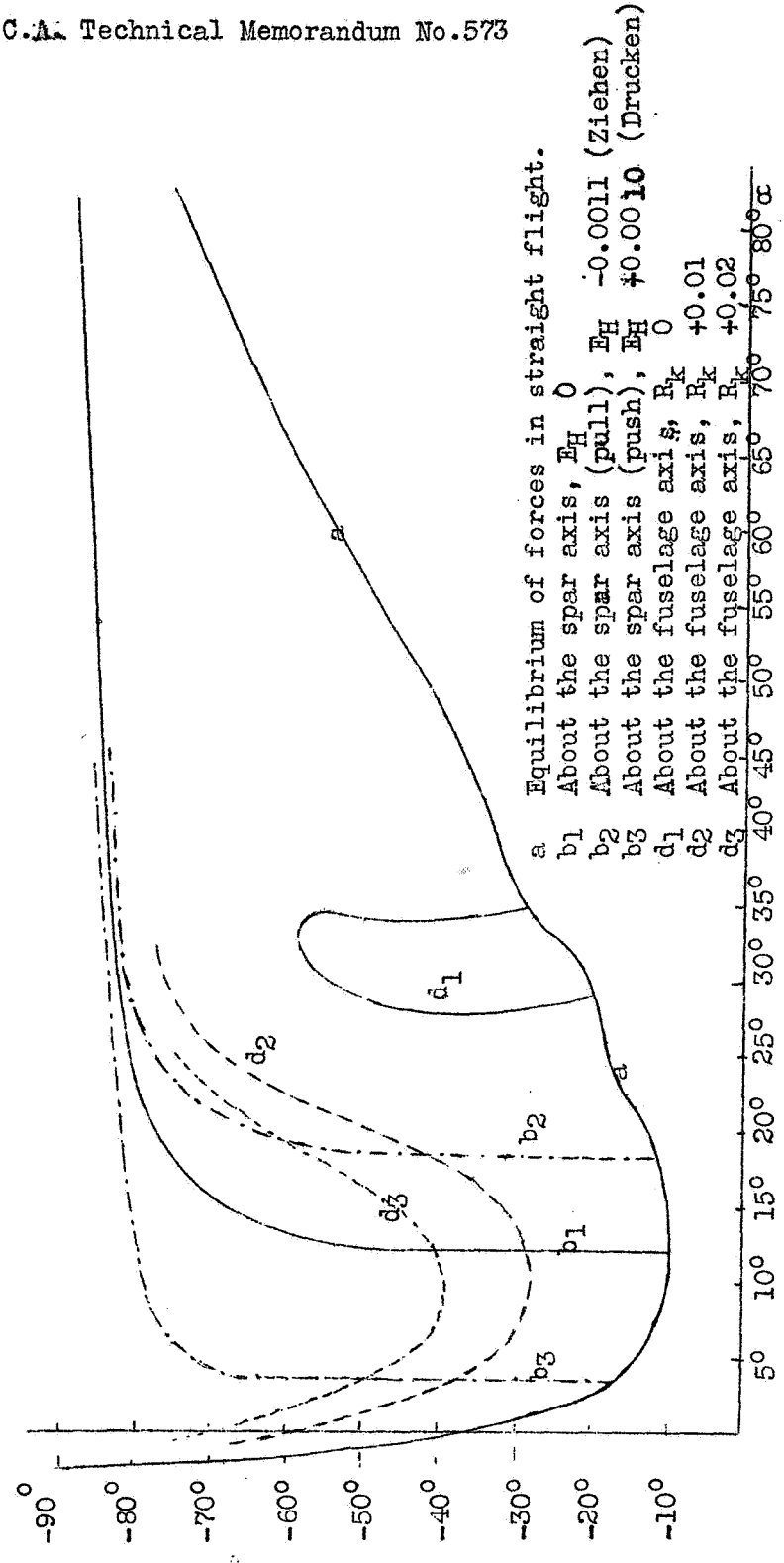

Fig.48 Equilibrium of the moments about the spar and fuselage axes of a Junkers type A 35 low-wing monoplane (original monoplane wing replaced by a single wing with auxiliary wing according to Fig.24) for different elevator and aileron moments and with all the forces about the airplane balanced. The angle of glide plotted against the angle attack.